SCIENTIFIC REPORTS

OPEN

Two-dimensional Turbulence in Symmetric Binary-Fluid Mixtures: Coarsening Arrest by the Inverse Cascade

Prasad Perlekar[1,*], Nairita Pal[2,*] & Rahul Pandit[2,3,*]

We study two-dimensional (2D) binary-fluid turbulence by carrying out an extensive direct numerical simulation (DNS) of the forced, statistically steady turbulence in the coupled Cahn-Hilliard and Navier-Stokes equations. In the absence of any coupling, we choose parameters that lead (a) to spinodal decomposition and domain growth, which is characterized by the spatiotemporal evolution of the Cahn-Hilliard order parameter ϕ, and (b) the formation of an inverse-energy-cascade regime in the energy spectrum $E(k)$, in which energy cascades towards wave numbers k that are smaller than the energy-injection scale $kin j$ in the turbulent fluid. We show that the Cahn-Hilliard-Navier-Stokes coupling leads to an arrest of phase separation at a length scale Lc, which we evaluate from $S(k)$, the spectrum of the fluctuations of ϕ. We demonstrate that (a) $Lc \sim LH$, the Hinze scale that follows from balancing inertial and interfacial-tension forces, and (b) Lc is independent, within error bars, of the diffusivity D. We elucidate how this coupling modifies $E(k)$ by blocking the inverse energy cascade at a wavenumber kc, which we show is $\simeq 2\pi/Lc$. We compare our work with earlier studies of this problem.

Binary-fluid mixtures (such as oil and water) have played a pivotal role in the development of the understanding of (a) equilibrium critical phenomena at the consolute point, above which the two fluids mix[1–3], (b) nucleation[4], and (c) spinodal decomposition, the process by which a binary-fluid mixture, below the consolute point and below the spinodal curve, separates into the two, constituent liquid phases until, in equilibrium, a single interface separates the two coexisting phases (this phase separation is also known as coarsening)[5,6]. In the presence of flows, the demixing because of spinodal decomposition gets arrested and an emulsion is formed. This process, also known as coarsening arrest, is important in several three-dimensional (3D) and two-dimensional (2D) turbulent flows. The former have been studied recently[7–9]. Coarsening arrest in a 2D, turbulent, binary-fluid mixture is also of relevance to problems such as the dynamics of oil slicks on the surface of the ocean, whose understanding is of clear socio-economic and scientific relevance[10–13]. Oceanic flows have been modelled successfully as 2D, turbulent fluids. Such 2D turbulence is fundamentally different from three-dimensional (3D) fluid turbulence as noted in the pioneering studies of Fjørtoft, Kraichnan, Leith, and Batchelor[14–18]. In particular, the fluid-energy spectrum in 2D turbulence shows (a) a *forward cascade* of enstrophy (or the mean-square vorticity), from the energy-injection wave number k_{inj} to larger wave numbers, *and* (b) an *inverse cascade* of energy to wave numbers smaller than k_{inj}. We elucidate the turbulence-induced arrest of phase separation in a 2D, symmetric, binary-fluid mixture.

Coarsening arrest by 2D turbulence has been studied in ref. 19, where it has been shown that, for length scales smaller than the energy-injection scale $\ell_{inj} = 2\pi/k_{inj}$, the typical linear size of domains is controlled by the average shear across the domain. However, the nature of coarsening arrest, for scales larger than ℓ_{inj}, i.e., in the inverse-cascade regime, which is relevant for large-scale oceanic flows, still remains elusive. In particular, it is not clear what happens to the inverse energy transfer, in a 2D binary-fluid, turbulent mixture, in which the mean size of domains provides an additional, important length scale. We resolve these two issues in our study. By combining theoretical arguments with extensive direct numerical simulations (DNSs) we show that the Hinze length scale L_H

[1]TIFR Centre for Interdisciplinary Sciences, 21 Brundavan Colony, Narsingi, Hyderabad 500075, India. [2]Centre for Condensed Matter Theory, Department of Physics, Indian Institute of Science, Bangalore 560012 India. [3]Jawaharlal Nehru Centre for Advanced Scientific Research, Jakkur, Bangalore, India. *These authors contributed equally to this work. Correspondence and requests for materials should be addressed to P.P. (email: perlekar@tifrh.res.in)

	N	ν	M	$\xi(\times 10^{-2})$	$\Lambda(\times \xi^2)$	D	$\langle f_\omega \omega \rangle$	E	ε_ν	ε_μ	We	Lc
R1	1024	10^{-4}	10^{-2}	1.76	1.0	10^{-2}	5.0	$3.3\cdot10^{-2}$	$2.5\cdot10^{-3}$	$5.7\cdot10^{-4}$	$5.9\cdot10^{-2}$	1.87
R2	1024	10^{-4}	10^{-4}	1.76	1.0	10^{-4}	5.0	$3.1\cdot10^{-2}$	$2.6\cdot10^{-3}$	$8.1\cdot10^{-4}$	$5.9\cdot10^{-2}$	1.87
R3	2048	10^{-4}	$2\cdot10^{-4}$	1.76	5.0	10^{-3}	5.0	$4.8\cdot10^{-2}$	$2.7\cdot10^{-3}$	$4.3\cdot10^{-4}$	$1.2\cdot10^{-2}$	2.97
R4	2048	10^{-4}	$1\cdot10^{-3}$	1.76	1.0	10^{-3}	5.0	$3.0\cdot10^{-2}$	$2.5\cdot10^{-3}$	$5.6\cdot10^{-4}$	$5.9\cdot10^{-2}$	1.82
R5	2048	10^{-4}	$2\cdot10^{-3}$	1.76	$5.0\cdot10^{-1}$	10^{-3}	5.0	$2.3\cdot10^{-2}$	$2.4\cdot10^{-3}$	$7.1\cdot10^{-4}$	$1.2\cdot10^{-1}$	1.35
R6	1024	10^{-4}	$4\cdot10^{-3}$	1.76	$2.5\cdot10^{-1}$	10^{-3}	5.0	$1.5\cdot10^{-2}$	$2.2\cdot10^{-3}$	$8.7\cdot10^{-4}$	$2.4\cdot10^{-1}$	0.9
R7	1024	10^{-4}	$8\cdot10^{-3}$	1.76	$1.25\cdot10^{-1}$	10^{-3}	5.0	$9.5\cdot10^{-3}$	$1.9\cdot10^{-3}$	$1.1\cdot10^{-3}$	$4.7\cdot10^{-1}$	0.57
R8	2048	10^{-4}	10^{-2}	1.76	$1.0\cdot10^{-1}$	10^{-3}	5.0	$8.1\cdot10^{-3}$	$1.8\cdot10^{-3}$	$1.2\cdot10^{-3}$	$5.9\cdot10^{-1}$	0.48
R9	2048	10^{-4}	$2\cdot10^{-4}$	0.50	5.0	10^{-3}	5.0	$3.7\cdot10^{-2}$	$2.8\cdot10^{-3}$	$3.4\cdot10^{-4}$	$4.1\cdot10^{-2}$	1.55
R10	2048	10^{-4}	10^{-3}	0.50	1.0	10^{-3}	5.0	$1.7\cdot10^{-2}$	$2.6\cdot10^{-3}$	$5.3\cdot10^{-4}$	$2.1\cdot10^{-1}$	0.63
R11	1024	10^{-2}	$2\cdot10^{-4}$	1.76	$5\cdot10^2$	10^{-1}	$4\cdot10^5$	$2.0\cdot10^1$	$2.4\cdot10^2$	$1.2\cdot10^1$	0.22	2.3
R12	1024	10^{-2}	10^{-3}	1.76	10^2	10^{-1}	$4\cdot10^5$	8.8	$2.0\cdot10^2$	$4.7\cdot10^1$	1.1	0.55

Table 1. Parameters N, ν, M, ξ, Λ, D, $\langle f_\omega \omega \rangle$ for our DNS runs R1-R12. The forcing wave number is fixed at $k_{inj} \equiv 2\pi/\ell_{inj} = 40$, N^2 is the number of collocation points, ν is the kinematic viscosity, M is the mobility parameter, ξ sets the scale of the interface width, the surface tension $\sigma = 2\sqrt{2}/3(\Lambda/\xi)$, $\langle f_\omega \omega \rangle$ is the enstrophy-injection rate, which is related to the energy-injection rate $[\varepsilon_{inj} = \langle f_\omega \omega \rangle / k_{inj}^2]$, $D \equiv M\Lambda/\xi^2$ is the diffusivity of our binary-fluid mixture, $E = 0.5\sum_k |u_k|^2$ is the fluid kinetic energy, $\varepsilon_\nu = \nu\sum_k k^2|u_k|^2$ is the fluid energy dissipation rate, $\varepsilon_\mu = M\sum_k k^2|\mu_k^2|$ is the energy dissipation rate because of the phase-field ϕ, $We \equiv \rho\varepsilon_{inj}^{2/3}\ell_{inj}^{5/3}/\sigma$, $Re \equiv u_{inj}\ell_{inj}/\nu$ is the Reynolds number, L_c is the coarsening-arrest length scale [Eq. (3)]. $R1-R2$: $Re = 124$ and $Sc = 1$; $R3-R10$: $Re = 124$ and $Sc = 0.1$; $R11-R12$: $Re = 53$ and $Sc = 0.1$. In some of our runs we also include a friction term $-\alpha\omega$ on the right-hand-side of Eq. (1); $\alpha = 0.001$ for runs $R4-R8$ and zero otherwise. In all our studies we use $k_{inj} = 40$ so that there is a clear separation between ℓ_{inj} and ξ.

(see refs 8,9) provides a natural estimate for the arrest scale; and the inverse flux of energy also stops at a wave-number scale $\simeq 2\pi/L_H$. Coarsening arrest has also been studied in simple shear flows (refs 20–25), which yield coarsening arrest with domains elongated in the direction of shear.

Forced, 2D, statistically steady, Navier-Stokes-fluid turbulence displays a forward cascade of enstrophy, from ℓ_{inj} to smaller length scales, and an inverse cascade of energy to length scales smaller than ℓ_{inj}. In the inverse-cascade regime, on which we concentrate here, $E(k) \sim k^{-5/3}$ (see, e.g., refs 15,18) and the energy flux $\Pi(k) \sim \varepsilon \equiv \langle \varepsilon(t) \rangle_t$ assumes a constant value. For the Cahn-Hilliard model, if it is *not* coupled to the Naiver-Stokes equation, $S(k, t) \sim \mathcal{S}(k\mathbb{L}(t))$, for large times, where the time-dependent length scale $\mathbb{L}(t) \sim t^{1/3}$, in the early Lifshitz-Slyozov[26–29] regime; if the Cahn-Hilliard model is coupled to the Navier-Stokes equation, then, in the absence of forcing, $\mathbb{L}(t) \sim t$, in the viscous-hydrodynamic regime, first discussed by Siggia[27–30], and $\mathbb{L}(t) \sim t^{2/3}$, in the very-late-stages in the Furukawa[31] and Kendon[32] regimes. For a discussion of these regimes and a detailed exploration of a universal scaling form for $\mathbb{L}(t)$ in 3D we refer the reader to ref. 33. We now elucidate how these scaling forms for $E(k)$ and $S(k, t)$ are modified when we study forced 2D turbulence, in the inverse-cascade regime in the coupled Cahn-Hilliard-Navier-Stokes equations.

Results

Cahn-Hilliard-Navier-Stokes equations.
We model a symmetric binary-fluid mixture by using the incompressible Navier-Stokes equations coupled to the Cahn-Hilliard or Model-H equations[34,35]. We are interested in 2D incompressible fluids, so we use the following stream-function-vorticity formulation[36–38] for the momentum equation:

$$(\partial_t + \boldsymbol{u}\cdot\nabla)\omega = \nu\nabla^2\omega - \nabla\times(\phi\nabla\mu) + f_\omega, \tag{1}$$

$$(\partial_t + \boldsymbol{u}\cdot\nabla)\phi = M\nabla^2\mu, \text{ and } \nabla\cdot\boldsymbol{u} = 0. \tag{2}$$

Here $\boldsymbol{u}(\boldsymbol{x}, t) \equiv (u_x, u_y)$ is the fluid velocity at the point $\boldsymbol{x}$ and time t, $\omega = (\nabla\times\boldsymbol{u})\hat{\boldsymbol{e}}_z$, $\phi(\boldsymbol{x}, t)$ is the Cahn-Hilliard order parameter that is positive in one phase and negative in the other, $p(\boldsymbol{x}, t)$ is the pressure, $\mu(\boldsymbol{x}, t) = \delta\mathcal{F}[\phi]/\delta\phi(\boldsymbol{x}, t)$ is the chemical potential, $\mathcal{F}[\phi] = \Lambda\int[(\phi^2 - 1)^2/(4\xi^2) + |\nabla\phi|^2/2]d\boldsymbol{x}$ is the free energy, Λ is the mixing energy density, ξ controls the width of the interface between the two phases of the binary-fluid mixture, ν is the kinematic viscosity, the surface tension $s = 2\sqrt{2}/3(\Lambda/\xi)$, the mobility of the binary-fluid mixture is M, and f_ω is the external driving force. For simplicity, we study mixtures in which M is independent of ϕ and both components have the same density and viscosity[33]. We use periodic boundary conditions in our square simulation domain, with each side of length $L = 2\pi$. To obtain a substantial inverse-cascade regime, we stir the fluid at an intermediate length scale by forcing in Fourier space in a spherical shell with wave-number $k_{inj} = 2\pi/\ell_{inj}$. Our choice of forcing $\hat{f}_\omega(\boldsymbol{k}, t) = \hat{\omega}(\boldsymbol{k}, t)/\sum_{k=k_{inj}}\hat{\omega}(\boldsymbol{k}, t)$, where the caret indicates a spatial Fourier transform, ensures that there is a constant enstrophy-injection rate. The higher the Reynolds number $Re \propto 1/\nu$, the more turbulent is the flow; and the higher the Weber number $We \propto 1/\sigma$, the more the fluctuations in the domains (see Table 1 for definitions of Re, We, and other parameters in our study). To elucidate the
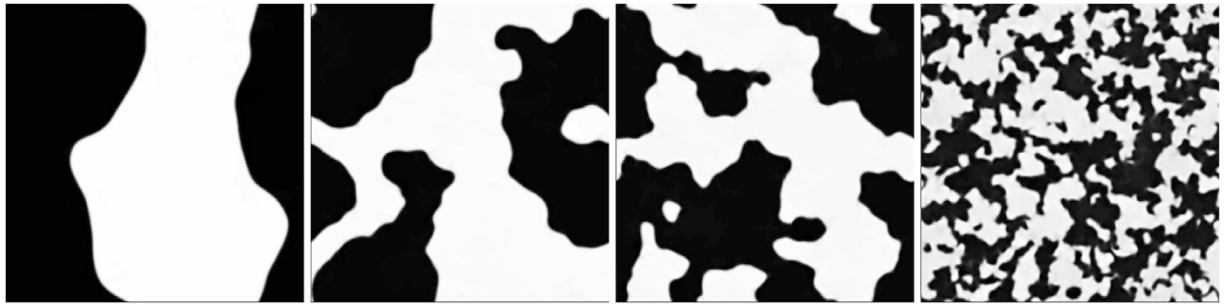
Figure 1. Pseudo-gray-scale plots of the order parameter field ϕ, at late times when coarsening arrest has occured, in 2D symmetric-binary-fluid turbulence with $Re = 124$. Note that the domain size decreases as we increase the Weber number We from the leftmost to the rightmost panel: $We = 1.2 \cdot 10^{-2}$ (R3); $We = 5.9 \cdot 10^{-2}$ (R4); $We = 1.2 \cdot 10^{-1}$ (R5); and $We = 5.9 \cdot 10^{-1}$ (R8).
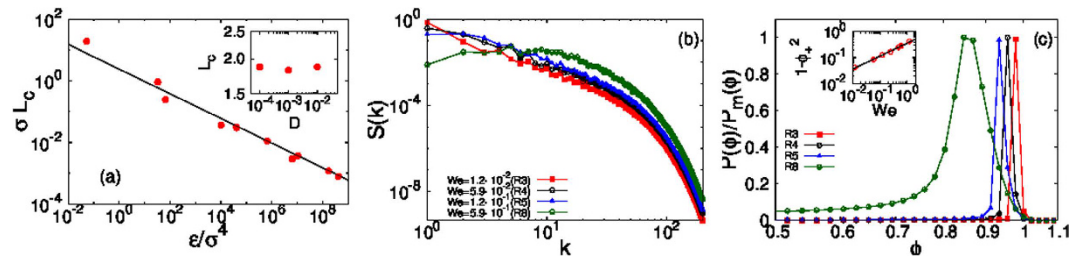

Figure 2. (**a**) Log-log (base 10) plot of σL_c versus ε/σ^4 showing data points (L_c from Equation (3), with $S(k)$ from our DNS) in red. The black line is the Hinze result (4) for L_H; a fit to our data yields a constant of proportionality $\simeq 1.6$ and an excellent approximation to the arrest scale L_c over several orders of magnitude on both vertical and horizontal axes; the plot of L_c versus D, in the inset, shows that, for fixed values of ε_ν and σ (runs R1, R2 and R4), L_c is independent of D (within error bars), as is implied by the Hinze condition (see text). (**b**) Log-log (base 10) plots of the spectrum $S(k)$, of the phase-field ϕ, versus k; as We increases (i.e., σ decreases) the low-k part of $S(k)$ decreases and $S(k)$ develops a broad and gentle maximum whose peak moves out to large values of k. (**c**) Plots versus ϕ, in the vicinity of the maximum at ϕ_+, of the normalized PDFs $P(\phi)/P_m(\phi)$, where $P_m(\phi)$ is the maximum of $P(\phi)$; the peak position $\phi_+ \to 1$ as We increases (see the inset which suggests that $1 - \phi_+^2 \sim We^{1/2}$ (black line)).

physics of coarsening arrest, we conduct direct numerical simulations (DNSs) of Eqs (1) and (2) (see Methods Section for details).

Coarsening Arrest. In Fig. 1 we show pseudo-gray-scale plots of ϕ, at late times when coarsening arrest has occurred, for four different values of We at $Re = 124$; we find that the larger the value of We the smaller is the linear size that can be associated with domains; this size is determined by the competition between turbulence-shear and interfacial-tension forces. This qualitative effect has also been observed in earlier studies of 2D and 3D turbulence of symmetric binary-fluid mixtures[19–21,39–44].

We calculate the coarsening-arrest length scale

$$L_c = 2\pi \left[\sum_k S(k) \right] \Big/ \left[\sum_k k S(k) \right]. \tag{3}$$

we now show that L_c is determined by the Hinze scale L_H, which we obtain, as in Hinze's pioneering study of droplet break-up[9], by balancing the surface tension with the inertia as follows:

$$L_H \sim \varepsilon_{inj}^{-2/5} \sigma^{3/5}. \tag{4}$$

We obtain for 2D, binary-fluid turbulence the intuitively appealing result $L_c \sim L_H$ (for a similar, recent Lattice-Boltzmann study in 3D see ref. 8). In particular, if we determine L_c from Eq. (3), with $S(k)$ from our DNS, we obtain the red points in Fig. 2, which is a log-log plot of σL_c versus $\varepsilon_{inj}/\sigma^4$; the black line is the Hinze result (4) for L_H, with a constant of proportionality that we find is $\simeq 1.6$ from a fit to our data. We see from Fig. 2 that the Hinze length scale L_H gives an excellent approximation to the arrest scale L_c *over several orders of magnitude on both vertical and horizontal axes*. Note that the Hinze estimate also predicts that, for fixed values of ε_{inj} and σ, the coarsening-arrest scale is independent of D; the plot of L_c versus D, in the inset of Fig. 2, shows that our data for L_c are consistent (within error bars) with this prediction.
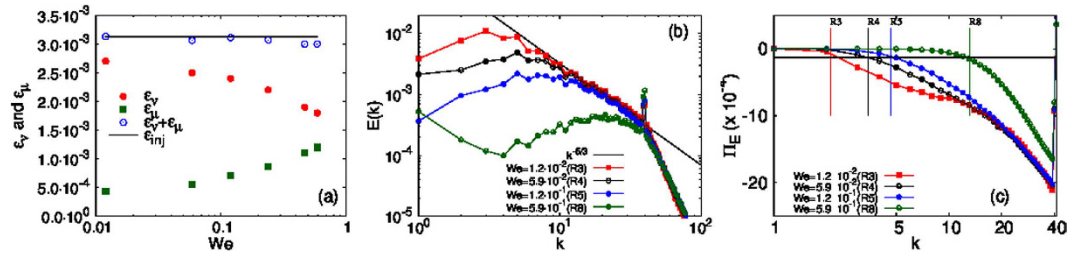
Figure 3. (**a**) Plots of the statistically-steady-state values of ε_ν, ε_μ, and their sum $\varepsilon_\nu + \varepsilon_\mu \simeq \varepsilon_{inj}$ versus We. (**b**) Log-log (base 10) plots of the energy spectrum $E(k)$ versus k, for different values of We, illustrating the truncation of the inverse energy cascade as We increases. The black line indicates the $k^{-5/3}$ result for the inverse-cascade regime in 2D fluid turbulence. (**c**) Log-log (base 10) plots of the energy flux $\Pi_E(k)$ versus k for different values of We. The intersection of the line $0.06\varepsilon_{inj}$ (black line) with $\Pi_E(k)$ gives k_c, the wave-number at which the inverse energy cascade gets truncated; our estimate of the arrest scale $2\pi/L_c$ (vertical lines) is comparable to k_c.

In Fig. 2(b) we show clearly how the arrest of coarsening manifests itself as a suppression of $S(k)$, at small k (large length scales). This suppression increases as We increases (i.e., σ decreases); and $S(k)$ develops a broad and gentle maximum whose peak moves out to large values of k as We grows. These changes in $S(k)$ are associated with We-dependent modifications in the probability distribution function (PDF) $P(\phi)$ of the order parameter ϕ, which is symmetrical about $\phi = 0$ and has two peaks at $\phi = \phi_\pm$, where $\phi_+ = -\phi_- > 0$; we display $P(\phi)/P_m(\phi)$ in Fig. 2(c) in the vicinity of the peak at ϕ_+; as We increases, ϕ_+ decreases; here $P_m(\phi)$ is the maximum value of $P(\phi)$. In particular, our DNS suggests that $1 - \phi_+^2 \sim We^{1/2}$, for small We.

The modification in $P(\phi)$ can be understood qualitatively by making the approximation that the effect of the fluid on the equation for ϕ can be encapsulated into an eddy diffusivity D_e[42,45,46]. The eddy-diffusivity-modified Cahn-Hilliard equation is $\partial_t \phi = (D_e - D)\nabla^2 \phi + D\nabla^2 \phi^3 + M\Lambda\nabla^4\phi$, which gives the maximum and minimum values of ϕ as $\phi_\pm = \sqrt{(D - D_e)/D}$. Furthermore, if we neglect the nonlinear term[27,29], we find easily that the modified growth rate is $Dk^2[(1 - D_e/D) - M\Lambda k^2]$; i.e., all wave numbers larger than $k_d = \sqrt{(1 - D_e/D)/(\Lambda M)}$ are stable to perturbations. In particular, droplets with linear size $<(2\pi/k_d)$ decay in the presence of coupling with the velocity field; we expect, therefore, that, in the presence of fluid turbulence, the peak of $P(\phi)$ broadens and shifts as it does in our DNS. For a quantitative description of this broadening and the shift of the peak, we must, of course, carry out a full DNS of the Cahn-Hilliard-Navier-Stokes equation as we have done here.

Energy spectrum. We have investigated, so far, the effect of fluid turbulence on the phase-field ϕ and its statistical properties such as those embodied in $S(k)$ and $P(\phi)$. We show next how the turbulence of the fluid is modified by ϕ, which is an *active* scalar insofar as it affects the velocity field. In the statistically steady state of our driven, dissipative system, the energy injection must be balanced by both viscous dissipation and dissipation that arises because of the interface, i.e., we must have $\varepsilon_{inj} = \varepsilon_\nu + \varepsilon_\mu$.

In Fig. 3(a), we show that ε_ν decreases and ε_μ increases as we increase We, while keeping ε_{inj} constant, because L_c diminishes (Fig. 1) and, therefore, the interfacial length and ε_μ increase. This decrease of L_c is mirrored strikingly in plots of the fluid-kinetic-energy spectrum $E(k)$ (Fig. 3(b)), which demonstrate that the inverse cascade of energy is effectively blocked at a wavenumber k_c, which we determine below, from the energy flux, and which we find is $\simeq 2\pi/L_c$, where L_c follows from $S(k)$ (see Fig. 2). The value of k_c increases with We; and the inverse cascade is completely blocked for the largest We we use, for which $k_c \simeq k_{inj}$, the forcing scale.

To provide clear evidence that the blocking of the energy flux is closely related to the arrest scale, we show in Fig. 3(c) plots of the energy flux $\Pi_E(k) = \int_k^\infty T(k')dk'$ for different values of We. Here $T(k) = \sum_{k-\frac{1}{2}\leq k'\leq k+\frac{1}{2}} \langle \hat{\boldsymbol{u}}(-\mathbf{k}, t) \cdot \mathbf{P}(\mathbf{k}) \cdot \widehat{(\boldsymbol{u} \times \boldsymbol{\omega})}(\mathbf{k}, t)\rangle_t$ is the energy transfer and $\mathbf{P}(\mathbf{k})$ is the transverse projector with components $P_{ij}(k) \equiv \delta_{ij} - k_ik_j/k^2$. We define k_c as the wave-number at which $\Pi_E(k)$ comes within 4% of ε_{inj}. We find that the wave-numer corresponding to the arrest scale $2\pi/L_c$ (marked by vertical lines for each run) is comparable to k_c.

In the presence of the standard viscous term $\nu\nabla^2\boldsymbol{u}$ and the Ekman drag $\alpha\boldsymbol{u}$, it is not possible to see a large range of constant energy flux[47,48]. However, it is possible to attain a large constant energy flux range by carrying out DNSs using hyperviscosity and hypoviscosity[47] (see the Methods Section for details). The plot in Fig. 4(left) shows the energy spectrum and the corresponding energy flux obtained [Fig. 4(right)] from our runs $HR1$ and $HR2$. Consistent with the earlier discussion, we find that the coarsening length L_c decreases on increasing We. Furthermore, the formation of arrest-scale domains leads to a blockage of the energy cascade; because we use hypoviscosity, we now see clear evidence of a constant energy flux over a decade for the single-phase Navier-Stokes run. For the binary-fluid case, the energy flux remains constant for a shorter range and then decreases to zero around a wave-number $\simeq 2\pi/L_c$.

Passive advection. It has been suggested[22,45,46] that coarsening arrest can be studied by using a model in which the field ϕ is advected passively by the fluid velocity. Such a passive-advection model is clearly inadequate because it cannot lead to the phase-field-induced modifications in the statistical properties of the turbulent fluid (see Fig. 3). The passive-advection case is easily studied by turning off the coupling term $\phi\nabla\mu$ in Eq. (2). We then contrast the results for this case with the ones we have presented above. The parameters we use for the
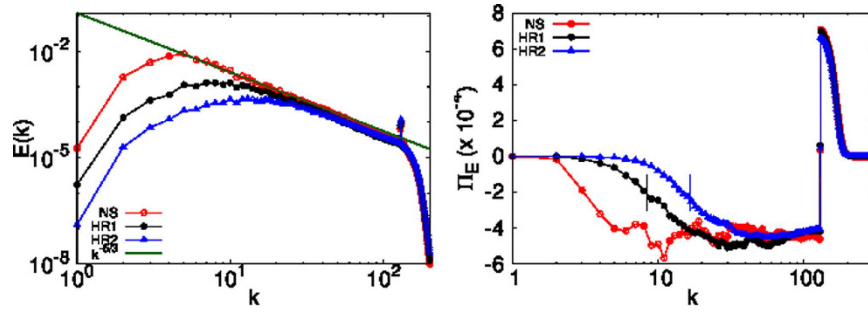
Figure 4. Log-log (base 10) plots of the kinetic energy spectrum $E(k)$ (left) and the corresponding energy flux $\Pi_E(k)$ for our runs $HR1: We = 1.7 \cdot 10^{-2}$ and $HR2: We = 4.3 \cdot 10^{-2}$. We also plot the single-phase Navier-Stokes energy spectrum and the energy flux for reference. On increasing We, small domains are formed and these lead to a truncation of energy flux at a wave-number around $\simeq 2\pi/L_c$ (marked by vertical lines).
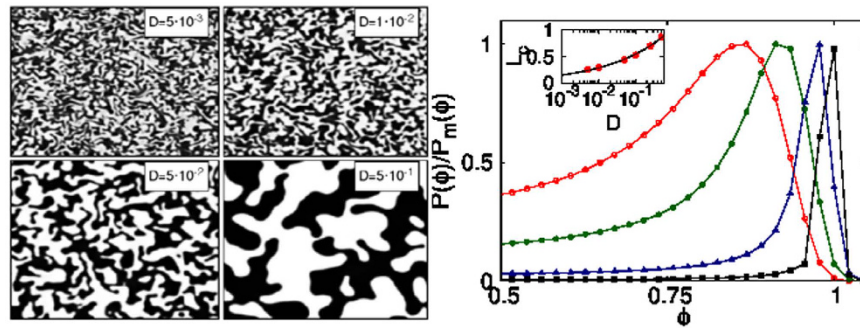

Figure 5. Passive-advection model: (Left panel) Pseudo-gray-scale plots of the order parameter ϕ for different values of the diffusivity D (cf. Fig. 1). (Right panel) Plots of $P(\phi)/P_m(\phi)$, in the vicinity of the maximum at ϕ_+ [cf. Fig. 2(c)];the inset shows that $L_c \sim D^{0.27}$ (black line), which is in stark contrast to the Cahn-Hilliard-Navier-Stokes result in the inset of Fig. 2(a).

passive-advection DNS are $N = 1024$, $\Lambda = \xi^2$, $\xi = 0.0176$; and we carry out runs for $D = 5 \cdot 10^{-3}$, $1 \cdot 10^{-2}$, $5 \cdot 10^{-2}$ and $5 \cdot 10^{-1}$. The evolution of the pseudo-grayscale plots of ϕ with D, in the left panel of Fig. 5, is qualitatively similar to the evolution shown in Fig. 1. There is also a qualitative similarity in the dependence on D of the scaled PDFs $P(\phi)/P_m(\phi)$; we can see this by comparing the passive-advection result, shown in the middle panel of Fig. 5 for positive values of ϕ in the vicinity of the peak, with its counterpart in Fig. 2(c). However, there is a qualitative difference in the dependence of L_c on D: in the passive-advection case we find $L_c \sim D^{0.27}$ [Fig. 5 (inset)], which is in stark contrast to the essentially D-independent behavior of L_c shown in the inset of Fig. 2(c).

Discussion

In conclusion, our extensive study of two-dimensional (2D) binary-fluid turbulence shows how the Cahn-Hilliard-Navier-Stokes coupling leads to an arrest of phase separation at a length scale L_c, which follows from $S(k)$. We demonstrate that $L_c \sim L_H$, the Hinze scale that we find by balancing inertial and interfacial-tension forces, and that L_c is independent, within error bars, of the diffusivity D. We also elucidate how the coupling between the Cahn-Hilliard and Navier-Stokes equations modifies the properties of fluid turbulence in 2D. In particular, we show that there is a blocking of the inverse energy cascade at a wavenumber k_c, which we show is $\simeq 2\pi/L_c$.

Earlier DNSs of turbulence-induced coarsening arrest in binary-fluid phase separation have concentrated on regimes in which there is a forward cascade of energy in 3D (see ref. 8) and a forward cascade of enstrophy in 2D (see ref. 19). Although studies that use a passive-advection model for ϕ obtain results that are qualitatively similar to those we obtain for $S(k)$ and the spatiotemporal evolution of ϕ, they cannot capture the phase-field-induced modification of the statistical properties of fluid turbulence and the correct dependence of L_c on D. We find our results to be in qualitative agreement with the earlier studies on the advection of binary-fluid mixtures with synthetic chaotic flows[45,46]; of course, such studies cannot address the effect of the phase field on the turbulence in the binary fluid.

Some groups have also studied the statistical properties of turbulent, symmetric, binary-fluid mixtures above the consolute point, where the two fluids mix even in the absence of turbulence[40,49,50]. In these studies, there is, of course, neither coarsening nor coarsening arrest.

We hope our study will lead to new experimental studies of turbulence in binary-fluid mixtures, especially in 2D[51-54], to test the specific predictions we make for L_c and the blocking of the inverse cascade of energy.

	N	ν_u	ν_i	M	ξ	$\Lambda(\times\xi^2)$	$\langle f_\omega\omega\rangle$	We	L_c
HR1	2048	10^{-35}	2.856	$1.0\cdot10^{-3}$	$4.42\cdot10^{-3}$	1.0	20	$1.7\cdot10^{-2}$	0.75
HR2	4096	10^{-35}	2.856	$2.5\cdot10^{-3}$	$2.21\cdot10^{-3}$	0.8	20	$4.3\cdot10^{-2}$	0.38

Table 2. Parameters N, ν_u, ν_i, M, ξ, Λ, $\langle f_\omega\omega\rangle$ for our DNS runs HR1 and HR2. The forcing wave number is fixed at $k_{inj}\equiv2\pi/\ell_{inj}=130$, N^2 is the number of collocation points, ν_u is the hyperviscosity, ν_i is the hypoviscosity, M is the mobility, parameter, ξ sets the scale of the interface width, the surface tension $\sigma=2\sqrt{2}/3(\Lambda/\xi)$, $\langle f_\omega\omega\rangle$ is the enstrophy-injection rate, which is related to the energy-injection rate $[\varepsilon_{inj}=\langle f_\omega\omega\rangle/k_{inj}^2]$, L_c is the coarsening-arrest length scale [Eq. (3)]. We also conduct a Navier-Stokes run with parameters the same as in run *HR1* for comparison.

Methods

Cahn-Hilliard-Navier-Stokes equations: Direct Numerical Simulations.
We conduct direct numerical simulations (DNSs) of Eqs (1) and (2) by using a Fourier pseudospectral method[55]; because of the cubic nonlinearity in the chemical potential μ, we use $N/2$-dealiasing. For time integration we use the exponential Adams-Bashforth method ETD2[56]. To obtain a substantial inverse-cascade regime, we stir the fluid at an intermediate length scale by forcing in Fourier space in a spherical shell with wave-number $k_{inj}=2\pi/\ell_{inj}$. Our choice of forcing $\hat{f}_\omega(\mathbf{k},t)=\hat\omega(\mathbf{k},t)/\sum_{k=k_{inj}}\hat\omega(\mathbf{k},t)$, where the caret indicates a spatial Fourier transform, ensures that there is a constant enstrophy-injection rate. The parameters for our DNSs are given in Table 1.

Given $\boldsymbol{u}(\boldsymbol{x},t)$ and $\phi(\boldsymbol{x},t)$ from our DNS, we calculate the energy and order-parameter (or phase-field) spectra, which are, respectively, $E(k)\equiv\sum_{k-\frac{1}{2}\le k'\le k+\frac{1}{2}}\langle|\hat{\boldsymbol{u}}(\mathbf{k}',t)|^2\rangle_t$ and $S(k)\equiv\sum_{k-\frac{1}{2}\le k'\le k+\frac{1}{2}}\langle|\hat\phi(\boldsymbol{k}',t)|^2\rangle_t$, where $\langle\rangle_t$ denotes the average over time in the statistically steady state of our system. The total kinetic energy is $E(t)=\frac{1}{2}\langle|\mathbf{u}(\boldsymbol{x},t)|^2\rangle_{\boldsymbol{x}}$ and the total enstrophy $\varepsilon(t)=\frac{1}{2}\langle|\omega(\boldsymbol{x},t)|^2\rangle_{\boldsymbol{x}}$, where $\langle\rangle_{\boldsymbol{x}}$ denotes the average over space, $\langle f_\omega\omega\rangle$ is the enstrophy-injection rate, which is related to the energy-injection rate via $\varepsilon_{inj}=\langle f_\omega\omega\rangle/k_{inj}^2$, $E=0.5\sum_k E(k)$ is the fluid kinetic energy, $\varepsilon_\nu=\nu\sum_k k^2 E(k)$ is the fluid-energy dissipation rate, and $\varepsilon_\mu=M\sum_k k^2\langle|\hat\mu(\mathbf{k},t)|^2|\rangle_t$ is the energy-dissipation rate because of the phase field ϕ.

Hyperviscous Cahn-Hilliard-Navier-Stokes equations.
The Cahn-Hilliard-Navier-Stokes equations with modified viscosity terms are[47]:

$$(\partial_t+\boldsymbol{u}\cdot\nabla)\omega=-\nu_i\nabla^{-4}\omega-\nu_u\nabla^{16}\omega-\nabla\times(\phi\nabla\mu)+f_\omega, \tag{5}$$

$$(\partial_t+\boldsymbol{u}\cdot\nabla)\phi=M\nabla^2\mu,\ \text{and}\ \nabla\cdot\boldsymbol{u}=0. \tag{6}$$

Here we use a hypo-viscosity term $-\nu_i\nabla^{-4}\omega$ to dissipate energy at large scales and a hyperviscosity term $-\nu_u\nabla^{16}\omega$ to dissipate enstrophy at small scales. As discussed in the main text, we use a constant-energy-injection forcing with $k_{inj}=130$. The other parameters for our simulations are given in Table 2.

References

1. Fisher, M. E. The theory of equilibrium critical phenomena *Rep. Prog. Phys.* **30,** 615 (1967).
2. Kumar, A. *et al.* Equilibrium critical phenomena in binary liquid mixtures *Phys. Rep.* **98,** 57 (1983).
3. Kardar, M. *Statistical Physics of Fields* (Cambridge University Press, UK, 2007).
4. Huang, J. S. *et al.* Homogeneous Nucleation in a Critical Binary Fluid Mixture *Phys. Rev. Lett.* **33,** 140 (1974).
5. Gunton, J. D. *et al.* In *Phase Transitions and Critical Phenomena* edited by Domb, C. & Lebowitz, J., Vol. 8, Chap. The Dynamics of First Order Phase Transitions, p. 269 (Academic Press, London, 1983).
6. Onuki, A. *Phase Transition Dynamics* (Cambridge University Press, UK, 2002).
7. Vankova, N. *et al.* Emulsification in turbulent flow: 1. Mean and maximum drop diameters in inertial and viscous regimes. *J. Colloid Interface Sci.* **312,** 363 (2007).
8. Perlekar, P. *et al.* Spinodal decomposition in Homogeneous and Isotropic Turbulence *Phys. Rev. Lett.* **112,** 014502 (2014).
9. Hinze, J. O. Fundamentals of the hydrodynamic mechanism of splitting in dispersion processes, *A.I.Ch.E. Journal* **1,** 289 (1955).
10. Olascoaga, M. J. & Haller, G. Forecasting sudden changes in environmental pollution patterns. *Proc. Natl. Acad. Sci.* **109,** 4738 (2012).
11. Wang, S. D. *et al.* Two-dimensional numerical simulation for transport and fate of oil spills in the seas. *Ocean Eng.* **32,** 1556 (2005).
12. Lehr, W. J. Review of modeling procedures for oil spill weathering behavior. *Advances in Ecological Sciences* **9,** 51 (2001).
13. Reed, M. *et al.* Oil spill modeling towards the close of the 20th century: Overview of the state of the art. *Spill Science and Technology Bulletin* **5,** 3 (1999).
14. R. Fjørtoft On the changes in the spectral distribution of kinetic energy for twodimensional, nondivergent flow. *Tellus* **5,** 226 (1953).
15. Kraichnan, R. H. Inertial ranges in two-dimensional turbulence. *Phys. Fluids* **10,** 1417 (1967).
16. Leith, C. Diffusion approximation for two-dimensional turbulence. *Phys. Fluids* **11,** 671 (1968).
17. Batchelor, G. K. Computation of the energy spectrum in homogeneous two-dimensional turbulence. *Phys. Fluids Suppl. II* **12,** 233 (1969).
18. Lesieur, M. *Turbulence in Fluids*, Vol. 84 of *Fluid Mechanics and Its Applications* (Springer, The Netherlands, 2008).
19. Berti, S. *et al.* Turbulence and coarsening in active and passive binary mixtures. *Phys. Rev. Lett.* **95,** 224501 (2005).
20. Hashimoto, T. *et al.* String phase in phase-separating fluids under shear flow. *Phys. Rev. Lett.* **74,** 126 (1995).
21. Onuki, A. Phase transitions of fluids in shear flow. *J. Phys. Condens. Matter* **9,** 6119 (1997).
22. Berthier, L. Phase separation in a homogeneous shear flow: Morphology, growth laws, and dynamic scaling. *Phys. Rev. E* **63,** 051503 (2001).
23. Stansell, P. *et al.* Nonequilibrium Steady States in Sheared Binary Fluids. *Phys. Rev. Lett.* **96,** 085701 (2006).
24. Stratford, K. *et al.* Binary fluids under steady shear in three dimensions. *Phys. Rev. E.* **76,** 030501(R) (2007).
25. Fielding, S. M. Role of inertia in nonequilibrium steady states of sheared binary fluids. *Phys. Rev. E* **77,** 021504 (2008).

26. Lifshitz, I. M. & Slyozov, V. V. The kinetics of precipitation from supersaturated solid solutions. *J. Phys. Chem. Solids* **19,** 35 (1959).
27. Bray, A. J. Theory of phase ordering kinetics. *Adv. Phys.* **43,** 357 (1994).
28. Puri, S. In *Kinetics of Phase Transitions* edited by Puri, S. & Wadhawan, V., Vol. 6, p. 437 (CRC Press, Boca Raton, US, 2009)
29. Cates, M. E. Complex fluids: The physics of emulsions. *Proceedings of the Les Houches Summer School on Soft Interfaces*, 2–27 July 2012 (Oxford University Press, Oxford, 2013).
30. Siggia, E. D. Late stages of spinodal decomposition in binary mixtures. *Phys. Rev. A* **20,** 595 (1979).
31. Furukawa, H. Effect of inertia on droplet growth in a fluid *Phys. Rev. A* **31,** 1103 (1985).
32. Kendon, V. M. Scaling theory of three-dimensional spinodal turbulence. *Phys. Rev. E* **61,** R6071 (2000).
33. Kendon, V. M. *et al.* Inertial effects in three-dimensional spinodal decomposition of a symmetric binary fluid mixture: a lattice Boltzmann study. *J. Fluid Mech.* **440,** 147 (2001).
34. Hohenburg, P. & Halperin, B. Theory of dynamic critical phenomena. *Rev. Mod. Phys.* **49,** 435 (1977).
35. Cahn, J. W. Spinodal Decomposition. *Trans. Metall. Soc. AIME* **242,** 166 (1968).
36. Perlekar, P. & Pandit, R. Statistically steady turbulence in thin films: direct numerical simulations with Ekman friction. *New Journal of Physics* **11,** 073003 (2009).
37. Pandit, R. *et al.* Statistical properties of turbulence: an overview. *Pramana* **73,** 179 (2009).
38. Boffetta, G. & Ecke, R. E. Two-dimensional turbulence *Ann. Rev. Fluid Mech.* **44,** 427 (2012).
39. Chan, C. K. *et al.* Light-scattering study of a turbulent critical binary mixture near the critical point. *Phys. Rev. A* **35,** *1756* (1987).
40. Ruiz, R. & Nelson, D. R. Turbulence in binary fluid mixtures. *Phys. Rev. A* **23,** 3224 (1981).
41. Pine, D. J. *et al.* Turbulent suppression of spinodal decomposition. *Phys. Rev. A* **29,** 308 (1984).
42. Aronovitz, J. A. & Nelson, D. R. Turbulence in phase-separating binary mixtures. *Phys. Rev. A* **29,** 2012 (1984).
43. Lacasta, A. M. *et al.* Phase separation dynamics under stirring. *Phys. Rev. Lett.* **75,** 1791 (1995).
44. Berthier, L. Phase separation in a chaotic flow. *Phys. Rev. Lett.* **86,** 2014 (2001).
45. Náraigh, L. Ó. & Thiffeault, J.-L. Bubbles and filaments: Stirring a cahn-hilliard fluid. *Phys. Rev. E* **75,** 016216 (2007).
46. Náraigh, L. Ó. *et al.* Flow-parametric regulation of shear-driven phase separation in two and three dimensions. *Phys. Rev. E* **91,** 062127 (2015).
47. Xiao, Z. *et al.* Physical mechanism of the inverse energy cascade of two-dimensional turbulence: a numerical investigation. *J. Fluid Mech.* **619,** 1 (2009).
48. Boffetta, G. & Musacchio, S. Evidence for the double cascade scenario in two-dimensional turbulence. *Phys. Rev. E* **82,** 016307 (2010).
49. Jensen, M. H. & Olesen, P. Turbulent binary fluids: A shell model study. *Physica D* **111,** 243 (1998).
50. Ray, S. S. & Basu, A. Universality of scaling and multiscaling in turbulent symmetric binary fluids. *Phys. Rev. E* **84,** 036316 (2011).
51. Muzzio, F. J. *et al.* Self-similar drop-size distributions produced by breakup in chaotic flows. *Phys. Rev. Lett.* **67,** 54 (1991).
52. Solomon, T. H. *et al.* Role of lobes in chaotic mixing of miscible and immiscible impurities. *Phys. Rev. Lett.* **77,** 2682 (1996).
53. Solomon, T. H. Chaotic mixing of a immiscible impurities in a two-dimensional flow. *Phys. Fluids* **10,** 342 (1998).
54. Solomon, T. H. *et al.* Lagrangian chaos and multiphase processes in vortex flows. *Commun Nonlinear Sci Numer Simul* **8,** 239 (2003).
55. Canuto, C. *et al. Spectral methods in Fluid Dynamics* (Spinger-Verlag, Berlin, 1988).
56. Cox, S. M. & Matthews, P. C. Exponential time differencing for stiff systems. *Journal of Computational Physics* **176,** 430 (2002).

Acknowledgements

Author Contributions
P.P. and N.P. conducted the simulations. P.P., N.P., and R.P. analyzed the results, wrote the manuscript text, prepared figures, and reviewed the manuscript.

Additional Information
Competing Interests: The authors declare no competing financial interests.

How to cite this article: Perlekar, P. *et al.* Two-dimensional Turbulence in Symmetric Binary-Fluid Mixtures: Coarsening Arrest by the Inverse Cascade. *Sci. Rep.* **7,** 44589; doi: 10.1038/srep44589 (2017).

Publisher's note: Springer Nature remains neutral with regard to jurisdictional claims in published maps and institutional affiliations.